CrystEngComm

Accepted Manuscript

ROYAL SOCIETY OF CHEMISTRY

www.rsc.org/crystengcomm

Journal Name

ARTICLE

Low- and high-temperature oxidation of $Mn_{1.5}Al_{1.5}O_4$ in relation to decomposition mechanism and microstructure†

Svetlana V. Cherepanova,[*a,b] Olga A. Bulavchenko,[a,b] Evgeny Yu. Gerasimov[a,b] and Sergey V. Tsybulya[a,b]

Spinel-like $Mn_{1.5}Al_{1.5}O_4$ is an unstable compound whose decomposition is induced by partial oxidation of Mn^{2+} ions in the temperature range of 300–800°C in air. According to XRD two spinel-like phases $Mn_{0.4}Al_{2.4}O_4$ and $Mn_{2.8}Al_{0.2}O_4$ are formed during both cooling and heating of $Mn_{1.5}Al_{1.5}O_4$. In this paper we have studied microstructural changes of $Mn_{1.5}Al_{1.5}O_4$ to understand the decomposition mechanism. During heating, low-temperature oxidation takes place and decomposition appears to be of the nucleation and growth of slightly Al-doped β-Mn_3O_4 nanoparticles on the surface of parent spinel. On contrary, cooling leads to the high-temperature oxidation that results preferably in spinodal decomposition and formation of alternating Mn- and Al-rich lamellas of nanosized thickness. The present study provides a fundamental reference for the nanostructure design of the Mn–Al–O system and probably some other ones subjected to oxidative decomposition.

Introduction

Manganese-containing oxide systems are of interest as catalysts for the reactions of total oxidation.[1-7] They have similar activities with noble-metal catalysts but, in contrast to the latter, are more stable at high temperatures and sufficiently less expensive.[8,9] A Mn-Al-O catalyst is activated by calcination at temperatures of 950÷1000°C, which causes a sharp increase in its activity.[3,10] Such thermal treatment leads to the formation of $Mn_{1.5}Al_{1.5}O_4$ that is not stable in air and is subject to decomposition.[11,12]

$Mn_{1.5}Al_{1.5}O_4$ oxide has a spinel-like structure with a general formula AB_2O_4, where A and B are tetrahedral and octahedral ions, respectively. Oxygen atoms form a face-centered-cubic lattice. In a normal spinel, atoms A are located at the tetrahedral sites, while atoms B are located at the octahedral sites. As earlier shown [13], $Mn_{1.5}Al_{1.5}O_4$ is a partially inversed spinel $(Mn_{0.7}Al_{0.3})[Mn_{0.8}Al_{1.2}]O_4$ in which about half of all Mn ions occupy the tetrahedral sites (shown by parentheses) and another part of Mn ions occupy the octahedral sites (shown by brackets). It is known that the octahedrally coordinated Mn^{3+} is a Jahn-Teller (JT) ion. It is in a degenerate electronic state and undergoes a tetragonal JT distortion that lowers the symmetry and thus removes the orbital degeneracy and reduces the state energy. At high temperatures, the distortion

is hidden due to very rapid random movements of bonds. However, the distortion reveals itself at lower temperatures. Therefore, cooling leads to transformation of a cubic spinel γ-Mn_3O_4 into a tetragonal spinel β-Mn_3O_4 (hausmannite). In $Mn_{3-x}A_xO_4$ (A = Zn, Ga, Mg, Fe, Co, Al, etc) solid solutions, the distortion induces the clustering of JT ions and phase decomposition, resulting in spatially separated regions with higher and lower concentrations of JT ions. By utilizing this tendency, it is possible to fabricate different types of nanostructures. For example, in $ZnMnGaO_4$ [14], $MgMn_{1.5}Fe_{0.5}O_4$ [15] and $Co_{0.6}Fe_{0.9}Mn_{1.5}O_4$ [16] the nano-checkerboard patterns are observed. In these spinels all Mn ions have the oxidation state 3+. $Mn_{1.5}Al_{1.5}O_4$, besides Mn^{3+}, contains Mn^{2+} ions that can change their oxidation state to Mn^{3+} under thermal treatment in air. Increase in quantity of JT ions can lead to phase, structure and microstructure transformations.

Therefore, $Mn_{1.5}Al_{1.5}O_4$ spinel is an interesting object in terms of investigating the decomposition process, the effect of different treatment conditions on decomposition mechanisms and micro/nanostructure of products. Earlier it was shown that $Mn_{1.5}Al_{1.5}O_4$ can be obtained by calcination of Mn and Al oxides at 1000°C in an inert atmosphere or in vacuum, it does not undergo changes during thermal treatments in the absence of air and is decomposed in air.[13,17]

The present investigation deals mainly with the $Mn_{1.5}Al_{1.5}O_4$ microstructure transformations during different thermal treatments and gives definite description of the decomposition mechanisms. For this purpose, such methods as transmission electron microscopy, X-ray photoelectron spectroscopy and thermal gravimetry were applied along with in situ X-ray diffraction.

a. *Boreskov Institute of Catalysis SB RAS, Lavrentieva Ave. 5, 630090 Novosibirsk, Russia. E-mail: svch@catalysis.ru; Fax: +7 (383)330-80-56; Tel: +7(383)3269597*
b. *Novosibirsk State University, Pirogova Str. 2, 630090 Novosibirsk, Russia.*
†Electronic Supplementary Information (ESI) available: methodology used for the determination of the composition of Mn-Al spinel-like oxides from the lattice constants. See DOI: 10.1039/x0xx00000x

Experimental

Sample preparation

$Mn_{1.5}Al_{1.5}O_4$ was prepared by co-precipitation of manganese and aluminum hydroxides from $Al(NO_3)_3$ and $Mn(NO_3)_2$ salts by a water solution of ammonia at pH = 10 while stirring at a rate of 550 rpm. The initial sample was dried at 70-80°C for 1 h and then calcined in air at 700°C for 4 h and in argon at 1000°C for 4 h. Sample quenching was made by rapid cooling at a rate of 10°C/sec.

Characterization

X-ray diffraction (XRD). A D8 Advance X-ray diffractometer (Bruker, Germany) was employed for XRD measurements. High-temperature studies were carried out with an HTK-16 X-ray chamber (Anton Paar, Austria). The diffraction patterns were recorded using CuK_α radiation. The lattice constants were refined using XRD patterns for the quenched samples with use of TOPAS program.[18] The content of manganese and aluminum ions in the mixed Mn-Al spinel-like oxides were found from refined lattice constants with use of the Vegard's plot (ESI†, Figure S1) constructed on the base of literature data[19] for γ-Al_2O_3, β-Mn_3O_4, Mn_2AlO_4 and $MnAl_2O_4$ (ESI†, Table S1). To test applicability of this approach for the determination of composition of segregated solid solutions we carried out Rietveld refinement of atomic parameters including occupancies (ESI†). Good correspondence between two approaches was received. Also the accuracy of the composition determination was estimated (ESI†).

Transmission Electron Microscopy (TEM). TEM images were obtained on a JEM-2010 microscope (JEOL, Japan) with a resolution of 1.4 Å. Digital treatments of TEM images were made with use of Digital Micrograph software (Gatan, South Korea). Energy dispersive X-ray (EDX) analysis was carried out using an energy dispersive spectrometer with a Si (Li) detector and an energy resolution of 130 eV. Energy calibration was carried out on a standard sample α-Al_2O_3 replaced on a copper substrate. Quantitative measurements of the cations ratio were performed with use of special software (EDAX, USA). Possible errors are not more than 2 at.% for each element.

X-ray Photoelectron Spectroscopy (XPS). XPS study was carried out using an ES-300 electron spectrometer (Kratos Analytical) with $MgK\alpha$ irradiation. The spectra were recorded in the 14 kVx14 mA working mode of the X-ray gun. The spectrometer was calibrated by a standard method relative to two lines, $Au4f_{7/2}$ and $Cu2p_{3/2}$. The spectra were calibrated against the shift of all registered lines by the value corresponding to electrostatic shift of the C1s peak. The chemical composition of catalysts was calculated from the integrated intensities of peaks taking into account the atomic sensitivity factors.

Thermogravimetry (TG). TG curves were collected under flow of air by means of NETZSCH STA 449C at a ramping rate of 10°C/min from 30 to 1000°C and from 1000°C to room temperature. For measurements, 50 mg of the sample was used.

Results and discussion

In situ XRD studies

The quenched $Mn_{1.5}Al_{1.5}O_4$ sample was stepwise heated in the XRD chamber from room temperature to 1000°C and then stepwise cooled. Rate of heating and cooling was 10°C/min. Figure 1a displays a set of XRD patterns collected during the heating. The increase in temperature leads to a gradual decrease in the intensity of diffraction lines for $Mn_{1.5}Al_{1.5}O_4$ and their full disappearance at T = 550°C. Broad peaks of the new phases are observed starting from T = 500°C. As the temperature is raised to 850°C, the broad peaks become smaller and the narrow peaks of the Mn-Al oxide with a cubic spinel structure appear again. A further heating to 1000°C leads to full disappearance of broad peaks and a simultaneous increase in the intensity of narrow peaks.

Figure 1b shows XRD data obtained during the stepwise cooling of $Mn_{1.5}Al_{1.5}O_4$ from 1000 to 300°C. At 950°C, very small narrow peaks of corundum appear. Weak broad lines of new phases start to appear at 900°C. A decrease in the temperature to 700°C leads to a drastic decrease in the intensity of narrow peaks and to an increase in the intensity of broad peaks. At 650°C, the narrow peaks disappear. A further cooling does not cause changes of the diffraction patterns.

Earlier[17] it was shown that the phase compositions of products of decomposition during heating and cooling are the same and represent cubic $Mn_{0.4}Al_{2.4}O_4$ and tetragonal $Mn_{2.8}Al_{0.2}O_4$ spinels. Nevertheless, as it is shown further, the decomposition mechanisms and microstructure are different. Let us consider first how the spinel composition changes and what transformations occur on the particle surface.

Ex-situ XRD results: changes of Mn-Al spinel composition during heating and cooling in air

To eliminate the thermal expansion effect, after calcination at a certain temperature, the sample was quenched and then XRD patterns were collected. Mn-Al spinel compositions were determined from refined lattice constants with use of Vegard's plot constructed as dependence of Vn on the content of Al ions x in $Mn_{3-x-y}Al_x\square_yO_4$ (ESI†, Figure S1). The volume and quantity of Al ions were normalized to 4 oxygen atoms. The lattice constant decreases from 8.285 to 8.040 Å as the temperature increases from 300 to 700–800°C (Table 1). Content of Al slightly increases from 1.5 to 1.6 (T=300–450°C), then sharply rises to 2.1 (T=500°C) and slower increases to 2.4 (T=700°C) (Figure 2). So it can be proposed that manganese ions gradually leave the cubic Mn-Al spinel structure. Peaks of hausmannite-like (tetragonal) spinel of $Mn_{2.8}Al_{0.2}O_4$ composition s appear at 500°C.

During cooling from 1000 to 800°C a little increase in the cubic lattice constants corresponds to the change in the composition from $Mn_{1.5}Al_{1.5}O_4$ to $Mn_{1.7}Al_{1.3}O_4$ (Table 1, Figure 2). So Al^{3+} ions leave the Mn-Al oxide structure. Such chemical composition corresponds to the phase diagram of the Mn-Al-O system.[20] Upon further cooling to T=650°C, the Mn-Al cubic spinel decomposes with formation of $Mn_{2.8}Al_{0.2}O_4$ and $Mn_{0.4}Al_{2.4}O_4$. Furthe cooling doesn't lead to the changes.

Table 1 The lattice constants of cubic and tetragonal Mg-Al spinel-like oxides and normalized unit cell volumes (Vn) under heating (H) or cooling (C).

T, ^{o}C	Cubic spinel		Tetragonal spinel	
	a, Å	Vn, Å^3	a, c, Å	Vn, Å^3
300 (H)	8.285(1)	71.1(1)	not observed	-
400 (H)	8.273(1)	70.8(1)	not observed	-
500 (H)	8.152(5)	67.7(1)	5.740(5), 9.44(1)	77.8(3)
600 (H)	8.10(1)	66.4(1)	5.737(5), 9.44(2)	77.7(3)
700 (H)	8.040(3)	65.0(1)	5.721(2), 9.47(1)	77.5(1)
800 (H)	8.040(2)	65.0(1)	5.721(6), 9.46(1)	77.4(3)
900 (H)	8.307(1)	71.7(1)	not observed	-
1000(H)	8.285(1)	71.1(1)	not observed	-
850 (C)	8.312(1)	71.8(1)	not observed	-
800 (C)	8.324(1)	72.1(1)	not observed	-
650 (C)	8.040(2)	65.0(1)	5.723(5), 9.44(2)	77.3(3)

XPS results: changes of the surface Mn:Al ratio

Using the XPS method we investigated the surface composition of the sample after thermal treatments in air. Full and Mn2p XPS spectra of initial sample, samples heated to 300 and 600°C as well sample cooled to 800°C are shown in the ESI† on the Figures S5 and S6 respectively. Figure 3 presents the ratio of Mn ions to Al ions on the surface. After the calcinations at 300 and 600°C, the Mn:Al ratio increases from 1.16 to 1.51 and 1.85, respectively. The initial Mn:Al ratio is higher than 1, which can be related to the beginning of Mn diffusion towards the surface as a result of oxidation at room temperature.

Similar effect was found for Fe-based spinels with composition $Fe_{3-x}Ti_xO_4$ synthesized using soft chemistry followed by thermal annealing under a reducing mixture of $N_2/H_2/H_2O$ gases.[21] Fe-segregation was found inside stoichiometric particles when the powders were studied ex situ; they exhibited strong surface iron enrichment. This heterogeneity authors relate to kinetic effects linked to the lower mobility of Ti^{4+} cations relative to Fe^{2+} ones during the partial oxidation of cations. The difference in cation mobility can be explained by a high valence of Ti^{4+} cations and consequently by strong connection to the oxygen anions.[22] In our case only Mn ions can change oxidation state and move toward the surface of particles.

During the cooling to 800°C, the Mn:Al ratio on the surface decreases from 1.16 to 0.9. This changes in the Mn:Al ratio are consistent with the XRD results, showing increase in Mn content in the volume of particles. So it can be proposed that mechanisms of oxidation of Mn^{3+} ions are different during heating and cooling.

For the identification of Mn oxidation states we considered the binding energy of Mn2p$_{3/2}$ peak that increases progressively as the oxidation state of Mn increases. According to the literature data[23-30] MnO, Mn_3O_4, Mn_2O_3 and MnO_2 are characterized by the Mn2p$_{3/2}$ binding energies in the range of 640.6–641.0, 641.2–641.5, 641.7–641.9 and 641.9–642.6 respectively. For all our measured samples the Mn2p$_{3/2}$ binding energy was 641.4–641.5 so it can be concluded that there is the mixture of Mn^{2+} and Mn^{3+} states.

TEM studies: microstructure of the samples heated to different temperatures and cooled in an oven

Thus, according to XRD and XPS data Mn ions diffuse from the volume of cubic spinel particles to their surface during heating. At lower temperatures T=300–450°C, peaks of the Mn-enriched phase are not observed on the XRD patterns. Therefore, we investigated the initial and calcined samples by TEM. The initial sample is a well-crystallized spinel with the particle size larger than 100 nm (Figure 4a) and composition Mn:Al=1 (Figure 4b), that agrees with the XRD data. On the micrographs of the samples calcined at 300-400°C (Figures 4c, e, f), one can see small hausmanite (β-Mn_3O_4)-like particles on the surface of large particles of parent spinel. Chemical and phase composition of surface particles is confirmed by the high Mn:Al ratio (Figure 4f) and by the set of interplane distances 4.8, 2.9, 2.5 Å(Figure 4d) close to the distances in tetragonal β-Mn_3O_4 (d_{101}=4.924Å, d_{200}=2.881Å, d_{211}=2.487Å). Size of hausmanite-like particles varies in the range of 5–10 nm and 10-20 nm for the samples calcined at 300°C and 400°C respectively. Small sizes of particles and small amount of them do not allow one to observe this hausmanite-like-phase in XRD patterns. According to TEM (Figure 4g) combined with EDX (Figure 4e), the sample calcined at 600°C also contain surface particles having very high Mn:Al ratio.

TEM data of the sample cooled from 950°C to room temperature are shown in Figure 5. The sample contains very large particles with the particle size larger than 100 nm (Figure 5a, b). Structure of these particles is not perfect. Increase of the scale in the place of imperfections (Figure 5b, upper left corner) shows stipple contrast that can mean alternation of domains having different composition (Figure 5c, d). Indeed EDX analysis indicates that these domains have different contents of Al and Mn (Figures 5e, f). It is difficult to determine the exact composition of domains, because the analyzed area is broader than domains. The same behaviour of solid solutions is often observed during the spinodal decomposition (SD). SD is a clustering reaction in a homogeneous supersaturated solution that is unstable against infinitesimal fluctuations in density or composition. Therefore, the solution spontaneously separates into two phases, starting with small fluctuations and proceeding with a decrease in the Gibbs energy without a nucleation barrier.[31]

TG data

Figure 6 demonstrates derivatives of the TG curves obtained during heating and cooling in air. Heating up to 300°C leads to a small weight loss that can be connected with the loss of adsorbed molecules. As the temperature is raised to 650°C the sample weight increases. During the further heating to 1000°C, a weight loss is observed. In all probability, an increase in the sample weight means that oxygen is added to the sample, whereas a decrease in its weight indicates oxygen loss. In its turn, oxygen addition to the sample or its loss indicates that oxidation or reduction takes place, respectively. Al^{3+} ion does not change the oxidation state, while Mn ions do.

A comparison of XRD and DTG data shows that during heating to 650°C the $Mn_{1.5}Al_{1.5}O_4$ decomposition is accompanied by oxygen addition and consequently by the oxidation of Mn^{2+} ions. Actually, one of the decomposition products, $Mn_{0.4}Al_{2.4}\square_{0.2}O_4$, contains cation vacancies (or an excess of oxygen ions). According to material balance 1 mol of $Mn_{1.5}Al_{1.5}O_4$ decomposed on the 0.59 mol of $Mn_{0.4}Al_{2.4}O_4$ and 0.45 mol of $Mn_{2.8}Al_{0.2}O_4$. Oxygen increment is ~0.16 mol that is about of 1.4 wt.%. This is in agreement with the amount of oxygen calculated from TG data (~1.5 wt.%) that additionally confirms the phase composition of decomposition products.[17] Each O^{2-} ion oxidizes two Mn^{2+} ions to Mn^{3+} ones so content of Mn^{3+} ions increases from 0.5 mol to ~0.8 mol. In the range of 650-1000°C the system loses oxygen and at 1000°C becomes monophase with the initial cubic spinel structure. This process is accompanied by reduction of manganese ions.

During cooling from 1000 to 850°C, the spinel catches oxygen according to DTG data and changes its composition by enrichment with Mn ions due to diffusion of Al ions to the surface of particles according to XRD and XPS data. The quantity of Mn^{3+} gradually increases. Further cooling leads to spinel decomposition. The rate of Mn oxidation (Figure 6) is slow down to ca. 750°C, and partial decomposition is observed on XRD patterns as the appearance of small peaks at 37° (Figure 1b). After cooling below 750°C the rate of Mn oxidation sharply increases, which accelerates the decomposition, and at 650°C the spinel is fully decomposed (Figure 1b). Amount of added oxygen during cooling from 1000°C calculated from TG data is about 1.5 wt.% as in the case of heating.

TEM studies: microstructure of the samples cooled in XRD chamber under control

According to TEM data, cooling in an oven leads to the spinodal decomposition (SD). However, along with the spinodally decomposed particles, separate hausmannite-like particles are also observed. It can be caused by uncontrolled cooling in an oven. SD is usually reached by quenching the system to well below the phase separation temperature and into the spinodal (i. e., unstable) region of the composition-temperature phase diagram.[32] A comparison of XRD and DTG data shows that $Mn_{1.5}Al_{1.5}O_4$ instability can be connected with partial oxidation of Mn^{2+} ions that takes place in the regions of two main peaks of oxygen addition on the DTG curves. So, the samples were cooled in XRD chamber under control of cooling conditions.

At first, the samples were rapidly cooled (10°C/sec) to the temperatures of 500 and 660°C that correspond respectively to the maxima of the low temperature (LT) and high temperature (HT) peaks on DTG curves (Figure 6). Then samples were isothermally annealed at these temperatures for 4 h and quenched.

The rapid cooling to 500°C with subsequent isothermal treatment leads to the decomposition and causes the formation of dispersed system (Figure 7a) where along with ultrafine grained decomposed products (Figure 7b) very large hausmannite-like particles (>100 nm) of elongated shape are observed (Figure 7c, d). It should be noted that such large particles are not observed after relatively slow heating (10°C/min) to the temperature 600°C. Appearance of very large β-Mn_3O_4-like particles can be explained by very fast oxidation of Mn^{2+} to Mn^{3+} that stimulates fast diffusion of manganese ions on the surface of parent spinel and fast growth of hausmannite-like particles. At the same time at the rapid cooling (10°C/sec) to 500°C it seems to be that there was no time to the formation of high content of nuclei as in the case of relatively slow heating so some of hausmannite-like particles have elongated shape.

As opposed to the LT oxidation that is responsible for the nucleation and growth mechanism of $Mn_{1.5}Al_{1.5}O_4$ decomposition the HT oxidation leads to the spinodal decomposition. TEM data of the sample rapidly cooled to 660°C show that particles have stripe contrast (Figure 8) which can be interpreted as lamellar domain microstructure formed as a result of SD. EDX analysis (Figure 8c) from selected area (Figure 8b) gives averaged chemical composition of such particles that is Mn:Al=1:1 as in initial $Mn_{1.5}Al_{1.5}O_4$ spinel. EDX analysis can not determine the exact composition of individual domain, because the analyzed area is broader than domains. So interplane distances were calculated for two different domains (Figure 8d). The values 5.0 and 4.6 Å are close to the interplane distances of β-Mn_3O_4 (d_{101}=4.924Å) and $Mn_{0.4}Al_{2.4}O_4$ (cubic spinel, a=8.04Å, d_{111}=4.642Å). Also Al-rich corundum-type particles can be found (Figure 8e, f). Small amount of corundum is registered by XRD (Figure 1b).

Also we cooled the samples down to 750 and 700°C, where the oxidation rate is lower than at 660°C. After that, the samples were isothermally treated for 4 hours and quenched. TEM data for both samples indicate the presence of large initial spinel particles and small Mn_3O_4 ones. The presence of small Mn_3O_4 particles testifies to spinel decomposition by the nucleation and growth mechanism. As for the initial spinel, along with the particles having a perfect structure (Figure 9a), the strained ones (Figure 9b) are observed in the sample cooled down to 750°C. Cooling to 700°C increases strains in the particles (Figures 9c,d). It seems to be that such strains are connected with structural rearrangement before spinodal decomposition.

A scheme (mechanism) of $Mn_{1.5}Al_{1.5}O_4$ oxidative decomposition due to heating and cooling in air

In our earlier XRD study[17], a scheme of $Mn_{1.5}Al_{1.5}O_4$ decomposition during heating and cooling was proposed; however, it concerned only phase changes. In both cases phase composition is represented by tetragonal $Mn_{2.8}Al_{0.2}O_4$ and cubic $Mn_{0.4}Al_{2.4}O_4$ spinels. Such composition is metastable because at temperatures below 900°C the stable phases are α-Mn_2O_3 and α-Al_2O_3.[20] New results allow us to propose a more detailed scheme (mechanism) of decomposition including microstructural transformations observed by TEM (Figure 10).

The TEM study revealed that $Mn_{1.5}Al_{1.5}O_4$ decomposition leads to the formation of nanoheterogeneous systems consisting of Mn-rich and Al-rich particles (heating) or lamellar

domains (cooling) that can be connected with low- or high-temperature partial Mn^{2+} oxidation, respectively.

It is evident that the low-temperature oxidation of Mn^{2+} ions below then 580°C leads to spinel decomposition by the growth and nucleation mechanism. Such type of decomposition is easily achieved during heating. Oxidation of Mn^{2+} to Mn^{3+} and diffusion of manganese ions towards the surface of parent spinel leads to the formation of hausmannite-like particles of $Mn_{2.8}Al_{0.2}O_4$ composition. Size of these particles gradually increases with the calcination temperature. According TEM observations particle size is about 5–10 nm and 10-20 nm after calcination at 300°C and 400°C respectively. In the volume of particles, the number of Mn ions gradually decreases and the initial cubic spinel-type structure transforms into a cation-deficient aluminum-rich cubic spinel-like structure with composition of $Mn_{0.4}Al_{2.4}O_4$. According XRD after full decomposition the average particle sizes were evaluated to be 20 and 50 nm for $Mn_{2.8}Al_{0.2}O_4$ and $Mn_{0.4}Al_{2.4}O_4$, respectively

As the temperature increases to 850°C, a cubic spinel-type structure of $Mn_{3-x}Al_xO_4$ (x ~ 1.5) composition is formed again. It occurs due to a loss of oxygen atoms and partial reduction of Mn^{3+} to Mn^{2+}.

The decomposition by growth and nucleation also occurs at quick enough cooling to a temperature in the region of low-temperature peak of Mn^{2+} ions oxidation. Rapid cooling is demanded to avoid high-temperature oxidation. In this case along with small hausmannite-like particles (~10nm) very large particles (>100 nm) of elongated shape are formed.

In the high-temperature region preferably the spinodal decomposition takes place that is possible only when octahedral sited Mn^{2+} ions are oxidized in the volume of particles. Spinodal decomposition starts when the amount of Mn^{3+} ions in octahedral sites becomes critical. Due to the collective Jahn-Teller effect, Mn^{3+} ions in octahedra are segregated, replacing Al^{3+} ions. This leads to the aggregation of ions of the same kind into domains. Thickness of these domains is about 5-10nm.

Comparison with oxidation of magnetite and titanomagnetite. Some analogy can be drawn between oxidation of Mn-Al spinel and magnetite as well as titanomagnetite. Magnetite Fe_3O_4 being inverse spinel $(Fe^{3+})[Fe^{2+}Fe^{3+}]O_4$ contains Fe^{2+} ions that can be oxidized to Fe^{3+} ones only in octahedral surrounding of oxygen and titanomagnetite – solid solution between magnetite and ulvospinel $(Fe^{2+})[Fe^{2+}Ti^{4+}]O_4$ – contains Fe^{2+} both in tetrahedrons and in octahedrons.

The oxidation of magnetite is a two-stage process: $Fe_3O_4 \rightarrow \gamma\text{-}Fe_2O_3 \rightarrow \alpha\text{-}Fe_2O_3$.[33] The first stage of magnetite oxidation produces maghemite $\gamma\text{-}Fe_2O_3$ having structural formula $(Fe^{3+})[Fe^{3+}Fe^{3+}_{2/3}\square_{1/3}]O_4$. Two thirds of the Fe^{2+} ions are oxidized to Fe^{3+} remaining in the octahedral sites and one third of the Fe^{2+} ions are oxidized on the surface by the mechanism assumed by Colombo et al.[34] Oxygen is adsorbed and ionized with electrons coming from the oxidation of Fe^{2+} to Fe^{3+}. This oxidation would cause a diffusion of iron ions from inside the crystals of magnetite towards the surface. The

structural and magnetic characterizations of iron oxide nanoparticles with sizes in the range 5–20 nm confirm that their composition evolves from the maghemite for small sizes (typically < 8nm) up to a core of rather stoichiometric magnetite surrounded by an oxidized shell for large sizes (> 12 nm) via a perturbed oxidized state for intermediate sizes.[35] Similar mechanism of low-temperature oxidation is observed for the Mn-Al spinel. Mn^{2+} ions are also oxidized and move towards the surface of parent spinel.

Titanomagnetite crystallizes at ~ 1300°C. It undergoes two main modes of oxidation. High-temperature (subsolidus) oxidation leads to the so-called oxy-exsolution that produces Fe- and Ti- rich phases such as magnetite- and ilmenite (FeTiO3)-like lamellas, respectively.[36,37] So phase-equilibrium studies in the Fe-Ti-O system permit determination of the temperature and oxygen fugacity of formation of coexisting pairs of magnetite and ilmenite in many rocks.[38] The other type of oxidation occurs at ~300°C and produces metastable defect spinel titanomaghemite containing octahedrally sited cation vacancies which balance excess positive charge due to oxidation of Fe^{2+} to Fe^{3+}.[39,40] So titanomagnetite as magnetite shows low-temperature single-phase oxidation. Such type of oxidation takes place for submarine basalts that are generally extruded on the sea floor and are quickly quenched. Basalts erupted in air generally undergo high-temperature oxidation during the initial cooling of the flow. Low-and high-temperature oxidation of titanomagnetites can be related to the diffusion and oxidation of octahedrally and tetrahedrally sited Fe^{2+} respectively.[41] It can be connected with the fact that octahedrally sited cations have a high diffusion rate, because chemical bonding in octahedral sites is ionic. However covalent bonding in tetrahedral sites leads to a very low diffusion rate.[42,43]

As for Mn-Al spinel TG data show that amount of oxygen added during heating and cooling is the same and equal to ~1.5 wt.%. Also either low- or high-temperature oxidation is observed depending on the conditions of thermal treatment (heating or cooling). So it seems to be that in our case only the Mn^{2+} ions in octahedral sites are oxidised. As well as for Fe^{2+} the availability for oxidation of Mn^{2+} ions in tetrahedral sites is much lower as compared to that of Mn^{2+} ions in octahedral sites.[44]

If we assume that Mn^{2+} ions in the initial spinel and in decomposition products prefer only tetrahedral sites as in galaxite that is normal spinel $(Mn^{2+})[Al^{3+}_2]O_4$ then we additionally confirm that oxidation of Mn^{2+} ions takes place only in octahedral sites. So $(Mn_{0.7}Al_{0.3})[Mn_{0.8}Al_{1.2}]O_4$ [13] can be rewritten as $(Mn^{2+}_{0.7}Al^{3+}_{0.3})[Mn^{2+}_{0.3}Mn^{3+}_{0.5}Al^{3+}_{1.2}]O_4$. After decomposition content of Mn^{2+} in tetrahedral sites in 0.59 mol $(Mn^{2+}_{0.4}Al^{3+}_{0.6})[Al^{3+}_{1.8}]O_4$ and 0.45 mol $(Mn^{2+})[Mn_{1.8}Al_{0.2}]O_4$ is ~0.7 and remained without changes. Content of Mn^{3+} situated in octahedrons after decomposition is ~0.8 and corresponds to the initial amount of Mn ions in octahedrons.

Comparison of oxidative and non-oxidative decomposition. Mechanisms of the non-oxidative decomposition are well known. Nucleation and growth can occur in the whole composition range of the miscibility gap (below binodal and

above spinodal). Spinodal decomposition operates inside the spinodal region which is limited by area close to centerline of the miscibility gap. To avoid following nucleation and growth the temperatures should be deeply below the phase separation temperature.[32] However, at very low temperatures phase separation may be kinetically hindered due to slow diffusion. Using these rules makes it possible to do some predictions about decomposition mechanism and correspondingly about microstructure of decomposed products. Let us consider non-oxidative decomposition of two mixed oxides having compositions close to the centerline of the miscibility gap.[45,46] Phase separation of $Co_{1.7}Fe_{1.3}O_4$ occurs at temperatures below 900^oC. Spinodal decomposition was confirmed at 600 °C by X-ray diffraction and transmission electron microscopy studies. But very long time of treatment at 600°C leads to the replacing spinodal decomposition by a nucleation and growth process. After annealing at 300 to 450 °C for a few hours, the spinodal transformation leading to two-phase spinels, one rich in iron and the other rich in cobalt, was not so evident but was clearly revealed by Raman spectroscopy and electrical measurements.[45] The phase diagram of Ru-Ce-O indicates that the solubility between RuO_2 and CeO_2 is very low at temperatures below 800^oC. It was shown that at 280 ^oC Ru-Ce-O represents a single-phase amorphous oxide with a retained driving force for the spinodal decomposition. At 450 ^oC, the driving force for the spinodal decomposition is released and $Ru_{0.6}Ce_{0.4}O_2$ decomposes into rutile-like Ru-rich and fluorite-like Ce-rich phases.[46]

As for oxidative decomposition, example of $Mn_{1.5}Al_{1.5}O_4$ spinel having composition close to centerline of miscibility gap shows that different types of nanostructured materials can be produced due to different decomposition mechanisms depending on the Mn^{2+} oxidation temperature.

Conclusions

The $Mn_{1.5}Al_{1.5}O_4$ spinel undergoes complex transformations under thermal treatment in air. Decomposition into cubic $Mn_{0.4}Al_{2.4}O_4$ and tetragonal $Mn_{2.8}Al_{0.2}O_4$ spinel-like phases during heating and cooling is caused by partial oxidation of Mn^{2+} ions.[17] In this paper we showed that microstructure of decomposed products is different and depends on the temperature. Low-temperature oxidation of Mn^{2+} ions induces their diffusion toward the surface of parent spinel-type particles with the formation of β-Mn_3O_4 containing small amount of Al. Evidently it occurs according to the nucleation and growth mechanism. High-temperature oxidation stimulates increase of octahedrally coordinated Mn^{3+} ions in volume that leads to their clustering inside particles due to collective JT effect and causes spinodal decomposition. It was shown that low- or high-temperature oxidation of Mn^{2+} takes place during heating and cooling of $Mn_{1.5}Al_{1.5}O_4$ spinel respectively.

Acknowledgements

References

1   J.T. Kummer, *Prog. Energy Combust. Sci.*, 1980, **6**, 177–199.
2   M.Ferrandon, J. Carno, S. Jaras and E. Bjornbom, *Appl. Catal.*, A 1999, **180**, 153.
3   P.G. Tsyrul'nikov, V.S. Sal'nikov, V.A. Drozdov, S.A. Stuken, A.V. Bubnov, E.I. Grigorov, A.V. Kalinkin and V.I. Zaikovskii, *Kinet. Catal.*, 1991, **32**, 387.
4   J. Carno, M. Ferrandon, E. Bjornbom and S. Jaras, *Appl. Catal.*, A 1997, **155**, 265.
5   M.C. Alvarez-Galvan, V.A.De La Pena O'Shea, J.L.G. Fierro and P.L.Arias, *Catalysis Commun.*, 2003, **4**, 223.
6   M.A. Baltanas, A.B. Stiles and J.R. Katzer, *Appl. Catal.*, 1986, **28**, 13.
7   C. Lahousse, A. Bernier, P. Grange, D. Delmon, H. Papaefthimiou, T. Ioannides and X.E. Verykios, *J. Catal.*, 1998, **178**, 214.
8   M.F.M. Zwinkels, S.G. Jaras, P.G. Menon and T.A. Griffin, *Catal. Rev.-Sci. Eng.*, 1993, **35**, 319.
9   R.J. Farrauto, M.C. Hobson, T. Kennelly and E.M. Waterman, *Appl. Catal.*, A 1992, **81**, 227.
10 P.G. Tsyrulnikov, S.V. Tsybulya, G.N. Kryukova, A.I. Boronin, S.V. Koscheev, T.G. Starostina, A.V. Bubnov and E.N. Kudrya, *J. Mol. Catal.*, A 2002, **179**, 213.
11 S.V. Tsybulya, G.N. Kryukova, T.A. Kriger and P.G. Tsyrul'nikov, P.G. *Kinet. Catal.*, 2003, **44**, 287.
12 T.A. Krieger, S.V. Tsybulya and P.G. Tsyrulnikov, React. Kinet. Catal. Lett., 2002, **75**, 141.
13 O.A. Bulavchenko, S.V. Tsybulya, S.V. Cherepanova, T.N. Afonasenko and P.G. Tsyrulnikov, *J. Struct. Chem.*, 2009, **50**, 474.
14 S. Yeo, Y. Horibe, S. Mori, C.M. Tseng, C.H. Chen, A.G. Khachaturyan, C.L. Zhang and S.-W. Cheong, *Appl. Phys. Lett.*, 2006, **89**, 233120.
15 C.L. Zhang, S. Yeo, Y. Horibe, Y.J. Choi, S. Guha, M. Croft, S.-W. Cheong and S. Mori, *Appl. Phys. Lett.*, 2007, **90**, 133123.
16 C.L. Zhang, C.M. Tseng, C.H. Chen, S. Yeo, Y.J. Choi and S.-W. Cheong, *Appl. Phys. Lett.*, 2007, **91** 233110.
17 O.A. Bulavchenko, S.V. Tsybulya, P.G. Tsyrul'nikov, T.N. Afonasenko, S.V. Cherepanova and E.Yu. Gerasimov, *J. Struct. Chem.*, 2010, **51**, 500.
18 TOPAS – Total Pattern Analysis System, Version 4.2, Bruker AXS.
19 JCPDS X-ray Crystallography Database.
20 E.H.L.J. Dekker and G.D. Rieck, *Z. Anorg. Allg. Chem.*, 1975, **417**, 69.
21 N. Guigue-Millot, Y. Champion, M.J. Hytch, F. Bernard, S. Begin-Colin and P. Perriat, *J. Phys. Chem.*, B 2001, **105**, 7125.
22 B.J. Gillot, *Solid State Chem.*, 1994, **113**, 163.
23 M. Oku, K. Hirokawa and S. Ikeda, J. Electron Spectrosc. Relat. Phenom., 1975, **7**, 465.
24 V. D. Castro and G. Polzonetti, J. Electron Spectrosc. Relat. Phenom., 1989, **48**, 117.
25 M. Oku and K. Hirokawa, J. Electron Spectrosc. Relat. Phenom., 1976, **8**, 475.
26 C. N. R. Rao, D. D. Sarma, S. Vasudevan and M. S. Hegde Proc. Royal Soc. London A, 1979, **367**, 239.
27 J. S. Foord, R. B. Jackman and G. C. Allen, Philos. Mag. A 1984, **449**, 657.
28 G. C. Allen, S. J. Harris, A. Jutson and J. M. Dyke, Appl. Surf. Sci., 1989, **37**, 111.

29 A. Wollner, F. Lange, H. Schmelz, H. Kniizinger, Appl. Catal. A, 1993, **94**, 181.
30 B.R. Strohmeier, D.M. Hercules, J. Phys. Chem., 1984, **88**, 4922.
31 J.B. Clark, J.W.Hastie, L.H.E. Kihlborg, R. Metselaar and M.M. Thackeray, *Pure & App. Chem.*, 1994, **66**, 577.
32 W.I. Goldburg, C.-H. Shaw, J.S. Huang and M.S. Pilant, *J. Chem. Phys.*, 1978, **68**, 484.
33 M.A. Gheith, *Amer. Jour. Sci.*, 1952, **250**, 677.
34 U. Colombo, G. Fagherazzi, F. Gazzarini, G. Lanzavecchia and G. Sironi, *Nature*, 1964, **202**, 175.
35 W. Baaziz, B.P. Pichon, S. Fleutot, Y. Liu, C. Lefevre, J.M. Greneche, M. Toumi, T. Mhiri and S. Begin-Colin, *J. Phys.Chem.*, C 2014, **118**, 3795.
36 D.H. Lindsley, *Carnegie Institution of Washington Year Book*, 1962, **61**, 100.
37 S.E. Haggerty, In *Oxide Minerals: Petrologic and Magnetic Significance*, Ed. D.H. Lindsley, Mineralogical Society of America, Washington, DC, 1991, chapter 5, 129-220.
38 A.F. Buddington and D.H. Lindsley, *J. Petrol.*, 1964, **5**, 310.
39 G.A. Waychunas, In *Oxide Minerals: Petrologic and Magnetic Significance*, Ed. D.H. Lindsley, Mineralogical Society of America, Washington, DC, 1991, chapter 2, 11-68.
40 C. Groschner, S. Lan, A. Wise, A. Leary, M.S. Lucas, C. Park, D.E. Laughlin, M. Diaz-Michelena and M.E. McHenry, *IEEE Trans. Magn.*, 2013, **49**, 4273.
41 B. Gillot, F. Jemmali, F. Chassagneux, C. Salvaing and A. Rousset, *J. Solid State Chem.*, 1982, **45**, 317.
42 J.B. Goodenough and A.L Loeb, *Phys. Rev.*, 1955, **98**, 391.
43 A. Rousset, L. Clerc, A.C. Vajpei, B. Gillot and F. Jemmali, *J. Therm.Anal.*, 1987, **32**, 845.
44 B. Gillot, M.E. Guendouzi, P. Tailhades and A. Rousset, *React. Solids*, 1986, **1**,139.
45 T.M.A. Bui, H. Le Trong, L.Presmanes, A.Barnabe, C.Bonninque and P. Tailhades, *CrystEngComm*, 2014, 16, 3359.
46 Y. Li, X. Wang, Y. Shao, D. Tang, B. Wu, Z. Tang and W. Lin, *Phys. Chem. Chem. Phys.*, 2015, **17**, 1156.

Journal Name
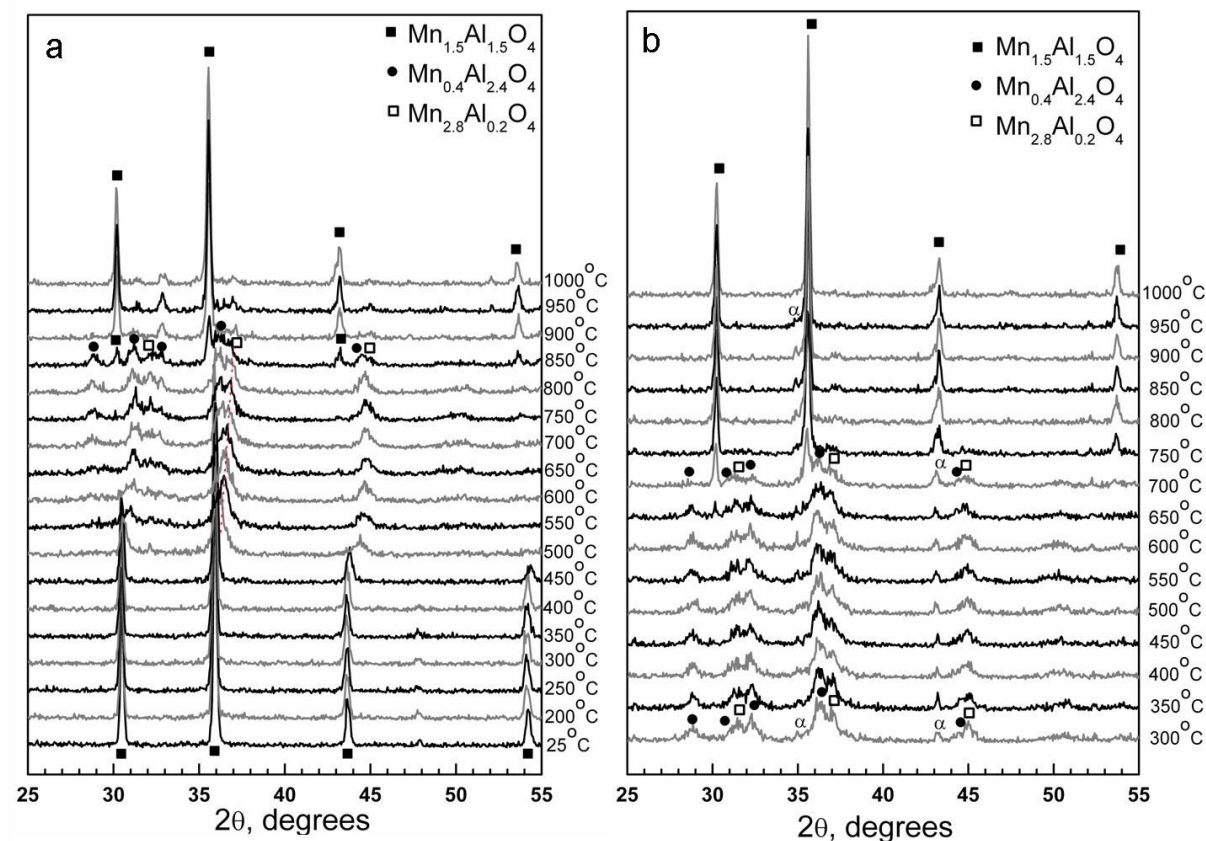
ARTICLE

Figures and Captions to the Figures

Fig. 1 In situ XRD patterns collected during thermal treatment of $Mn_{1.5}Al_{1.5}O_4$ in air: stepwise heating (a); stepwise cooling (b). α means corundum.
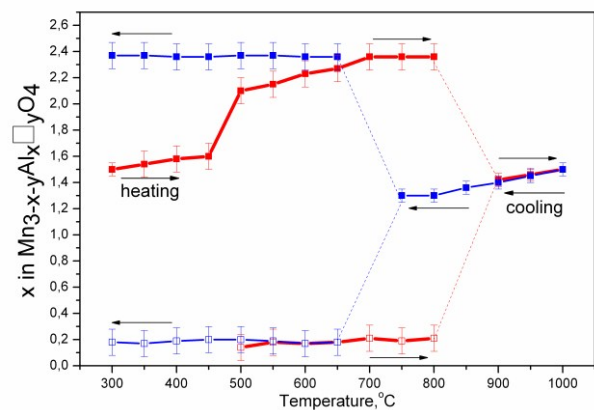
Fig. 2 Al content in Mn-Al spinel-like oxides as a function of the calcination temperature (according to ex-situ XRD data).
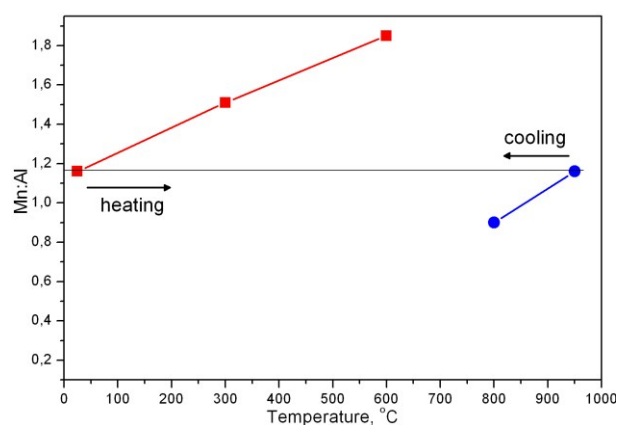

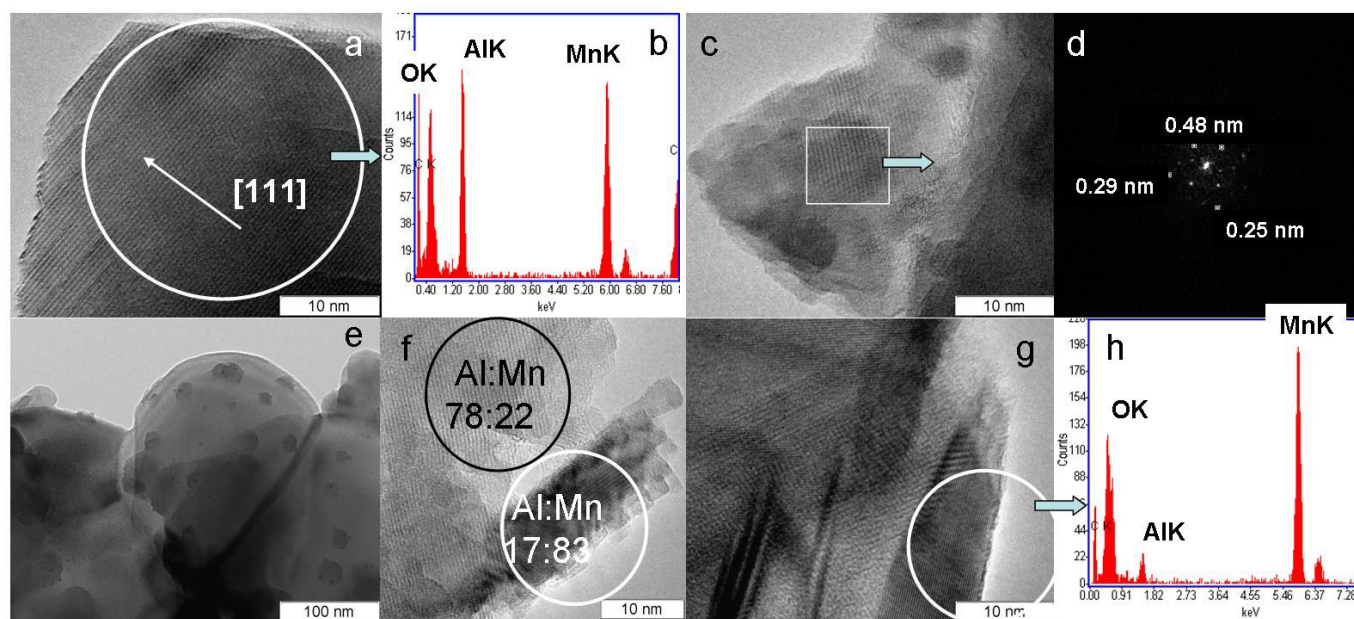**Fig. 3** The Mn:Al ratio on the surface of particles as a function of the calcination temperature (according to XPS data).

Fig. 4 TEM images of samples: initial Mn$_{1.5}$Al$_{1.5}$O$_4$ (a) with EDX analysis (b); calcined at 300°C (c) with FFT image (d); calcined at 400°C (e, f) with Al:Mn ratio calculated from EDX analysis (f); calcined at 600°C (g) with EDX analysis (h).
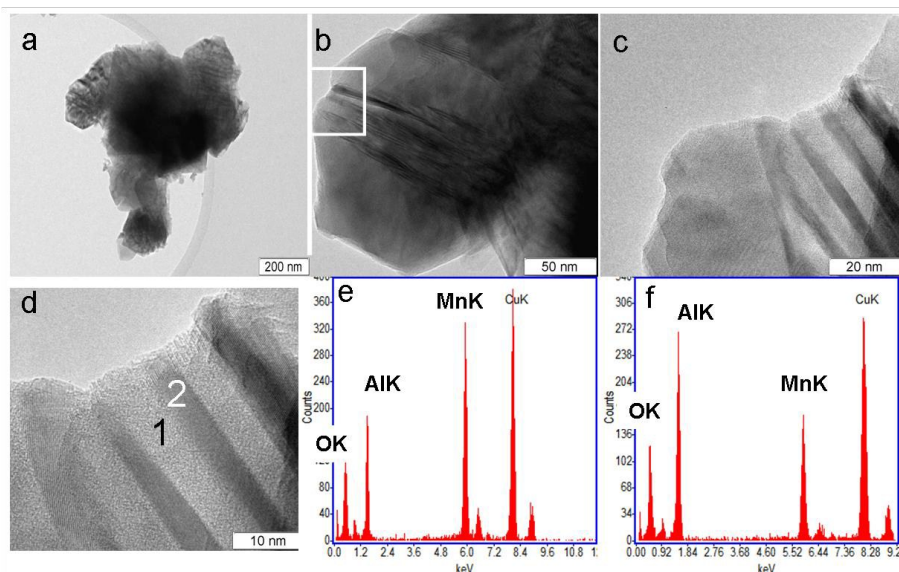
Fig. 5 TEM images of the sample cooled from 950°C to room temperature: general view (a, b); region with domain structure (c, d) with EDX analysis of selected regions 1 (e) and 2 (f).
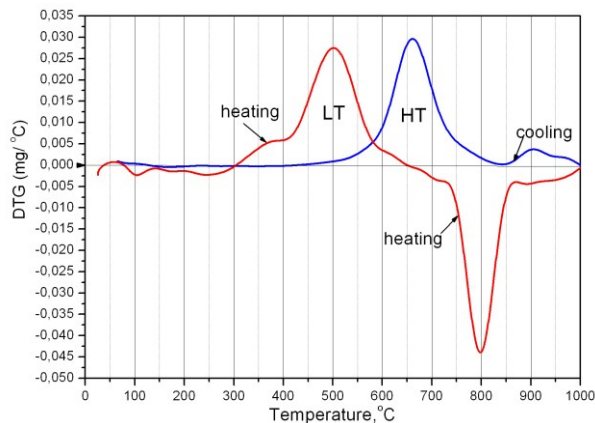
Fig. 6 DTG curves during heating (red line) and cooling (blue line) of Mn$_{1.5}$Al$_{1.5}$O$_4$.
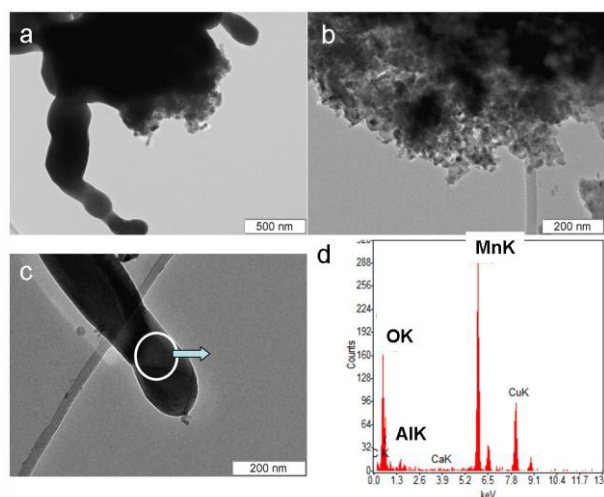
Fig. 7 TEM images of the sample rapidly cooled to 500°C: general view (a); region of small particles (b); large Mn-rich particle (c) with EDX analysis (d).
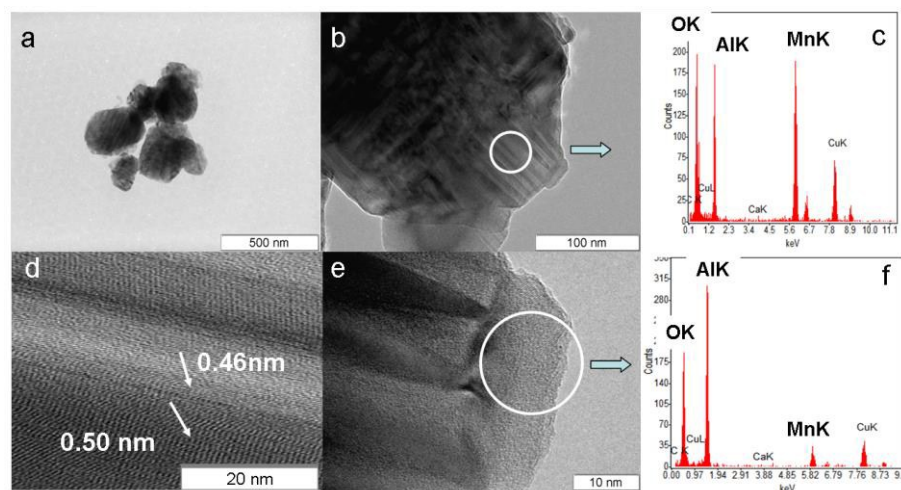

Fig. 8 TEM images of the sample rapidly cooled to 660°C: general view (a); region with domain structure (b) with EDX (c); domain structure, interplane distances are shown for each domain(d), domain structure and corundum-like particle (e) with EDX analysis(f);
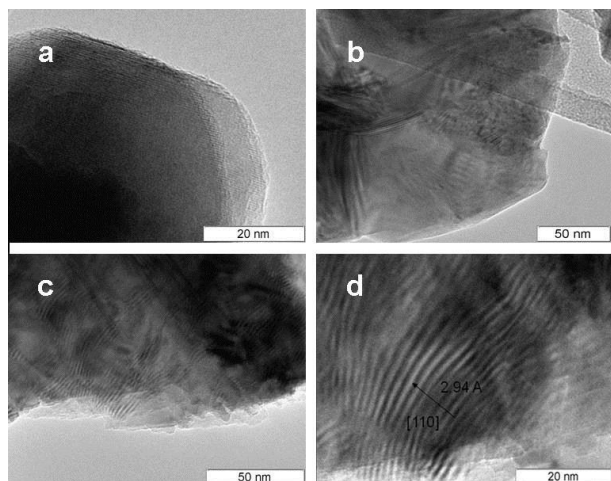
Fig. 9 TEM images for the sample rapidly cooled to 750°C (a, b); 700°C (c, d).
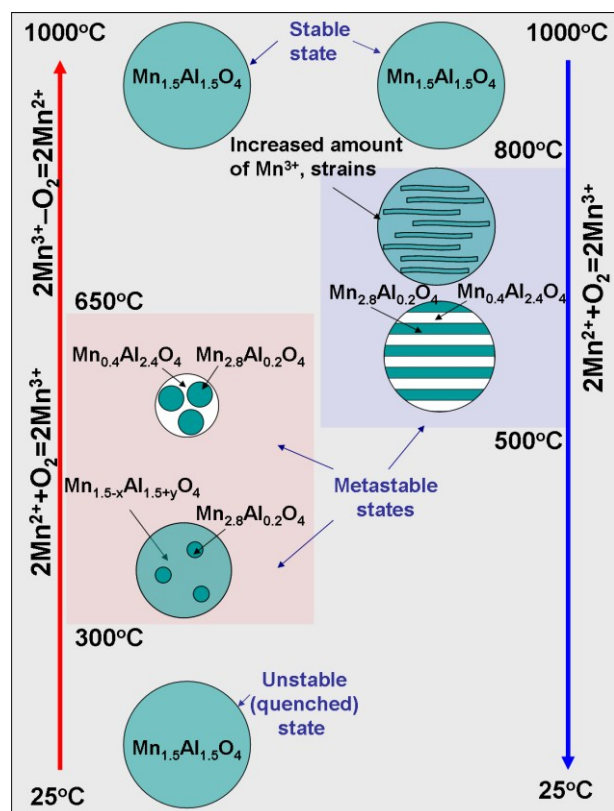

Fig. 10 Proposed scheme of $Mn_{1.5}Al_{1.5}O_4$ decomposition in air during heating (left) and cooling (right) due to partial oxidation of Mn^{2+} to Mn^{3+}. Heating leads to the diffusion of Mn ions on the surface, gradual enrichment of parent spinel by Al, nucleation and growth of hausmannite-like $Mn_{2.8}Al_{0.2}O_4$ particles on the surface. Size of surface particles is in the range of 5–10 nm at 300°C and 10-20 nm at 400°C. After full decomposition parent spinel has chemical composition $Mn_{0.4}Al_{2.4}O_4$ and average crystallite size ~50 nm. Average crystallite size of $Mn_{2.8}Al_{0.2}O_4$ is about 20 nm. Cooling down to 700°C leads to the increase of Mn^{3+} ions in the volume of particles

ARTICLE

and appearance of large strains. At 660°C spinodal decomposition takes place. As a result lamellar domains of $Mn_{2.8}Al_{0.2}O_4$ and $Mn_{0.4}Al_{2.4}O_4$ composition are formed. Thickness of domains is in the range of 5-10 nm.
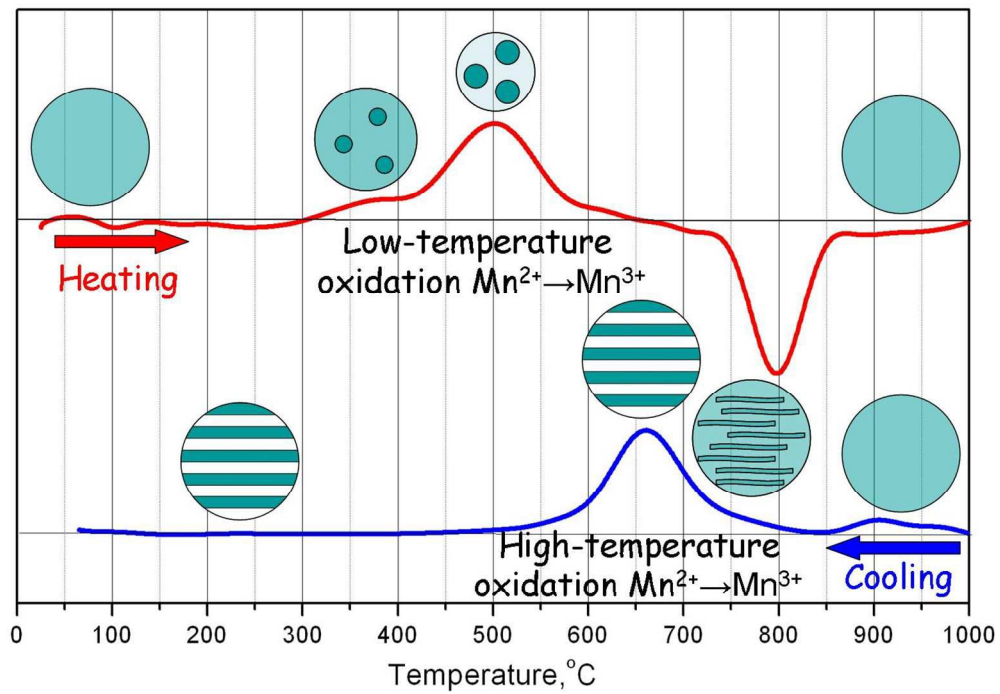
Partial oxidation of Mn^{2+} ions at different temperatures leads to the $Mn_{1.5}Al_{1.5}O_4$ decomposition and formation of different microstructures
254x177mm (150 x 150 DPI)